



Trans. Nonferrous Met. Soc. China 34(2024) 1321-1332

Transactions of Nonferrous Metals Society of China

www.tnmsc.cn



# Mechanism of lithium adsorption by AlLi-LDH with Al-O octahedral ring

Yong-pan TIAN, Cheng-cheng WANG, Fan ZHANG, Liang XU, Zhuo ZHAO, Bi-hai TONG School of Metallurgical Engineering, Anhui University of Technology, Ma'anshan 243032, China

Received 21 September 2022; accepted 14 February 2023

**Abstract:** Aluminum—lithium layered double hydroxide (AlLi-LDH) was synthesized using a co-precipitation method for Li<sup>+</sup> adsorption. AlLi-LDH crystallized in space group of *P*32 or *C*2/*m*, where the microstructure had regular spherical shapes with diameters of 5–10 μm. The space group of AlLi-LDH only belonged to *P*32 after Li<sup>+</sup> adsorption. The Li<sup>+</sup> adsorption from a solution with a Li<sup>+</sup> concentration of 95.4 mg/L reached 8.98 mg/g after 1 h. The adsorption amount increased to 16.50 mg/g after 48 h, where the Li<sup>+</sup> adsorption capacity determined by applying the second-order adsorption model was 17.57 mg/g. The Mg<sup>2+</sup>/Li<sup>+</sup> separation coefficient was 29536 when the mass ratio of Mg<sup>2+</sup> to Li<sup>+</sup> was 1067. The interaction strength of Li–O was weaker for AlLi-LDH in the *P*32, where the interaction occurs via the electrostatic effect. The Li<sup>+</sup> adsorption and desorption occurred more readily in AlLi-LDH belonging to *P*32 space group.

Key words: co-precipitation; aluminum-lithium layered double hydroxide; space group; adsorption; lithium

## 1 Introduction

Lithium has attracted considerable attention in recent years because of the rapid development of lithium batteries [1–3]. Salk lake brines are the most important lithium resources, where approximately 70% of industrially available lithium resources are contained in brines around the world. The main cations in salt lake brines are Na<sup>+</sup>, Mg<sup>2+</sup>, K<sup>+</sup>, Li<sup>+</sup>, Ca<sup>2+</sup>, etc [4–7]. Lithium can be separated from solution by membrane processes, liquid–liquid extraction, adsorption, electrochemical methods, and so on [8–10]. Among these methods, adsorption can be used to separate lithium from salt-lake brines with low energy consumption.

As adsorbent materials, lithium—alumina layered double hydroxides (AlLi-LDH) can simultaneously absorb Li<sup>+</sup> and anions [11,12]. Moreover, the desorption of lithium can be achieved using hot water, which avoids pollution of the salt-lake brine generated by the acid washing

process. The general chemical formula of AlLi-LDH is LiX·2Al(OH)<sub>3</sub>·nH<sub>2</sub>O, where X represents Cl<sup>-</sup>, OH<sup>-</sup>, CO<sub>3</sub><sup>2-</sup>, SO<sub>4</sub><sup>2-</sup>, etc. The side view of layers is shown in Fig. 1(a). Water molecules and anions are distributed between layers [13]. As shown in Fig. 1(b), the Al3+ cation is surrounded by six hydroxyl groups in an octahedral arrangement, and these octahedra share edges to form sheets [14,15]. Li<sup>+</sup> is surrounded by the Al-O octahedral arrangement. Some of the lithium ions can be washed out, and the vacancies can selectively adsorb lithium ions. The structure of AlLi-LDH was previously studied using Rietveld refinement of the X-ray and neutron powder diffraction patterns with Fullprof [16]. The sheets of AlLi-LDH form two different stacking structures: hexagonal and rhombohedral [17-19]. Many researchers have studied the efficacy of AlLi-LDH for separating lithium from impurity ions. PARANTHAMAN et al [20], reported that AlLi-LDH preferred to adsorb Li+, and the selectivity coefficients of Li<sup>+</sup>/Na<sup>+</sup> and Li<sup>+</sup>/K<sup>+</sup> were 47.8 and 212, respectively.

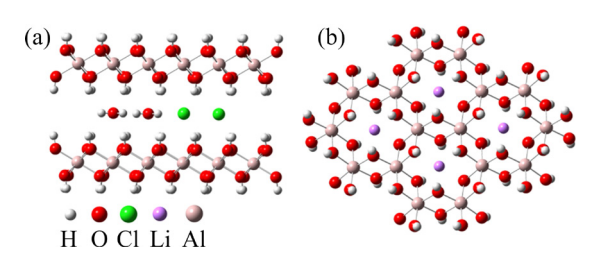


**Fig. 1** Crystal structure of AlLi-LDH: (a) Side view of layers; (b) Top view of layers

Fe-doped AlLi-LDH was synthesized by LI et al [21], and the adsorption experiments showed that the material had an adsorption selectivity to Li<sup>+</sup> with the ion-selective sequence of Li<sup>+</sup>>>Mg<sup>2+</sup>> Na<sup>+</sup>>K<sup>+</sup>>Ca<sup>2+</sup>. It is difficult to separate Li<sup>+</sup> from Mg<sup>2+</sup> since the Mg<sup>2+</sup>/Li<sup>+</sup> ratio of salt lakes in China can be more than 1000 [22–25]. ZHONG et al [11] showed that the Li<sup>+</sup> adsorption capacity of AlLi-LDH was 4.92 mg/g and the Mg<sup>2+</sup>/Li<sup>+</sup> mass ratio declined from 301.58 to 0.99 after the adsorption process. The effectiveness of LDH-doped Fe<sub>3</sub>O<sub>4</sub> materials for the Li<sup>+</sup> adsorption was studied by CHEN et al [26], where the adsorption capacity was approximately 5.83 mg/g, and the Mg<sup>2+</sup>/Li<sup>+</sup> ratio decreased from 284.00 to 2.10.

The Mg<sup>2+</sup>/Li<sup>+</sup> ratio of the solution for separation experiments was 1067 in this work. The relationship between the adsorption capacity and space group of AlLi-LDH was investigated. AlLi-LDH was synthesized via a co-precipitation method using lithium hydroxide and sodium aluminate solutions. X-ray powder diffraction (XRD), Le Bail refinement analysis, and X-ray photoelectron spectroscopy (XPS) were used to study the structural characteristics of the products. The microscopic morphologies of the materials were analyzed using scanning electron microscopy (SEM) and transmission electron microscopy (TEM). An LDH cluster model was established, and the independent density gradient analysis method (IGM) was used to study the interaction between lithium and oxygen atoms using Multiwfn [27-29]. The results of this study can be used as a guide for constructing AlLi-LDHs with a high capacity for Li<sup>+</sup>.

## 2 Experimental

### 2.1 Synthesis of AlLi-LDH

Analytically pure reagents (LiOH·H<sub>2</sub>O, NaOH,

and NaAlO<sub>2</sub>) were used to synthesize AlLi-LDH. Sodium aluminate solution was prepared using NaOH and NaAlO<sub>2</sub>. The concentration of aluminum in the sodium aluminate solutions was measured on the basis of Al<sub>2</sub>O<sub>3</sub> ( $\eta_{AO}$ ); the concentrations were 80, 100, and 150 g/L, respectively. The concentrations of LiOH were 18.82, 23.53, and 35.29 g/L, respectively. To synthesize AlLi-LDH, the lithium hydroxide and sodium aluminate solutions were mixed using a constant flow pump. The molar ratio of Li<sup>+</sup>:Al<sup>3+</sup>:OH<sup>-</sup> was 1:2:7. When lithium hydroxide solution was dropped into the sodium aluminate solution, the product was defined as P1. When sodium aluminate solution was dropped into the lithium hydroxide solution, the product was defined as P2. The solution was mixed and stirred for 3 min at room temperature, after which the product was aged in the mixed solution for 8 h at 80 °C. The synthesized AlLi-LDH was washed to neutrality with hot water and then dried at 80 °C for 2 h.

## 2.2 Structural analysis

XRD data were collected using a Shimadzu XRD-6000 diffractometer with Cu K<sub>α1</sub> radiation  $(\lambda_{Cu}=1.54056 \text{ Å})$ . The data were recorded in the  $2\theta$ range of 5°-90°. The phase compositions of the products were determined by Jade using the database PDF2-2004. During analysis, background was subtracted using the cubic spline method. Le Bail fitting was performed using Fullprof to analyze the structural characteristics of AlLi-LDH. XPS was also used to investigate the interactions between the Al, O, and Li atoms using Thermo Scientific K-Alpha. The microscopic morphology of the products was analyzed using Shimadzu SSX-550 and FEI Tecnai instruments. Analysis and visualization of the AlLi-LDH clusters were carried out using Multiwfn3.6 and Visual Molecular Dynamics [30,31].

## 2.3 Adsorption performance

Analytical reagent (AR) grade lithium chloride and magnesium chloride were used for the separation experiments; the pH of the mixed solution was 6.80. The adsorption experiments were carried out in a thermostatic water-bath at 25 °C with a stirring speed of 200 r/min. The mass ratio of Mg<sup>2+</sup> to Li<sup>+</sup> was calculated according to Eq. (1). Equations (2) and (3) were used to obtain the partition and separation coefficients. The adsorption

amount was calculated according to Eq. (4). The adsorption kinetics were studied using the Li+ adsorption experiments with P1-LDH in a pure lithium solution. The adsorption time varied from 10 min to 48 h. The initial Li<sup>+</sup> concentration was 1.00 g/L. The mass of P1-LDH was 2 g, and the volume of solution was 100 mL during the adsorption process. The adsorption data were studied using pseudo-first-order and pseudosecond-order models according to Eqs. (5) and (6). Inductively coupled plasma-optical emission spectroscopy (ICP-OES) was used to measure the ion concentration.

$$\beta_{\rm Mg^{2+}}^{\rm Li^{+}} = \frac{m_{\rm mg^{2+}}}{m_{\rm Li^{+}}} \tag{1}$$

$$K_{\rm d} = \frac{\left(c_0 - c_{\rm e}\right)V}{c_{\rm e}m} \tag{2}$$

$$\alpha_{\rm Mg^{2+}}^{\rm Li^{+}} = \frac{K_{\rm d}^{\rm Li}}{K_{\rm d}^{\rm Mg}} \tag{3}$$

$$q_t = \frac{V(c_0 - c_t)}{m} \tag{4}$$

$$\ln(q_e - q_t) = \ln q_e - k_1 t \tag{5}$$

$$\frac{t}{q_t} = \frac{1}{k_2 q_e^2} + \frac{1}{q_e} t \tag{6}$$

where  $\beta_{\mathrm{Mg}^{2+}}^{\mathrm{Li}^+}$  is the mass ratio of Mg<sup>2+</sup> to Li<sup>+</sup>;  $m_{\mathrm{mg}^{2+}}$  is the mass of Mg<sup>2+</sup> in solution;  $m_{\mathrm{Li}^+}$  is the mass of Li<sup>+</sup> in solution;  $c_0$  and  $c_{\mathrm{e}}$  (mg/L) are the initial and equilibrium concentrations of the metal ion in solution, respectively; V (mL) is the volume of solution; m (g) is the mass of AlLi-LDH;  $K_{\mathrm{d}}$  is the partition coefficient;  $\alpha_{\mathrm{Mg}^{2+}}^{\mathrm{Li}^+}$  is the separation coefficient of Mg<sup>2+</sup>/Li<sup>+</sup>;  $c_t$  (mg/L) is the residual cation concentration in the solution at time t;  $q_{\mathrm{e}}$  (mg/g) is the adsorption equilibrium state;  $q_{\mathrm{t}}$  (mg/g) is the adsorption amount at time t;  $k_{\mathrm{l}}$  and  $k_{\mathrm{l}}$  are the adsorption constants.

## 3 Results and discussion

#### 3.1 Characteristics of AlLi-LDH crystal structure

There are three types of ions in the sodium aluminate solution: Na<sup>+</sup>, OH<sup>-</sup>, and aluminate anions. Common aluminate anions are Al(OH)<sub>4</sub><sup>-</sup>,

 $Al(OH)_6^{3-}$ , and  $Al(OH)_8^{5-}$ . The transformations among different aluminate anions are shown in Eqs. (7) and (8). The Al(OH)<sub>3</sub> formation processes are shown in Eqs. (9), (10), and (11). Equations (12), (13) and (14) show the formation of AlLi-LDH during the solution-mixing process. The Al(OH)<sub>3</sub> and AlLi-LDH formation processes are shown in Eqs. (15), (16), and (17). The XRD patterns of P1 and P2 are shown in Figs. 2 and 3, respectively. Based on the comparison with the characteristic peaks of cards 81-1573, 31-0704, 77-0250, and 72-0623, P1 contained only AlLi-LDH and P2 contained both Al(OH)3 and AlLi-LDH. Therefore, Al(OH)<sub>3</sub> and AlLi-LDH were simultaneously formed when sodium aluminate solution was dropped into the lithium hydroxide solution. When the lithium hydroxide solution was dropped into the sodium aluminate solution, the transformations among the aluminate anions may prevent the formation of Al(OH)3. Thus, P1 contains only AlLi-LDH. The phase compositions of P1 and P2 do not change after the Li<sup>+</sup> adsorption when  $\eta_{AO}$ was 80, 100, and 150 g/L, respectively.

$$Al(OH)_4^- + 2OH^- = Al(OH)_6^{3-}$$
 (7)

$$Al(OH)_6^{3-} + 2OH^- = Al(OH)_8^{5-}$$
 (8)

$$Al(OH)_4^- - OH^- = Al(OH)_3$$
 (9)

$$Al(OH)_6^{3-} - 3OH^- = Al(OH)_3$$
 (10)

$$Al(OH)_8^{5-} - 5OH^- = Al(OH)_3$$
 (11)

$$Li^{+} + 2Al(OH)_{4}^{-} + 2H_{2}O =$$
[LiAl<sub>2</sub>(OH)<sub>6</sub>]OH·2H<sub>2</sub>O+OH<sup>-</sup> (12)

$$\text{Li}^{+} + 2\text{Al}(\text{OH})_{6}^{3-} + 2\text{H}_{2}\text{O} =$$

$$[\text{LiAl}_{2}(\text{OH})_{6}]\text{OH} \cdot 2\text{H}_{2}\text{O} + 5\text{OH}^{-}$$
(13)

$$\text{Li}^+ + 2\text{Al}(\text{OH})_8^{5-} + 2\text{H}_2\text{O} =$$

$$[\text{LiAl}_2(\text{OH})_6]\text{OH} \cdot 2\text{H}_2\text{O} + 9\text{OH}^-$$
(14)

$$Li^{+} + 3Al(OH)_{4}^{-} + 2H_{2}O =$$
[LiAl<sub>2</sub>(OH)<sub>6</sub>]OH·2H<sub>2</sub>O+Al(OH)<sub>3</sub>+2OH<sup>-</sup> (15)

$$\text{Li}^+ + 3\text{Al}(\text{OH})_6^{3-} + 2\text{H}_2\text{O} =$$
 $[\text{LiAl}_2(\text{OH})_6]\text{OH} \cdot 2\text{H}_2\text{O} + \text{Al}(\text{OH})_3 + 8\text{OH}^- \quad (16)$ 

$$\text{Li}^+ + 3\text{Al}(\text{OH})_8^{5-} + 2\text{H}_2\text{O} =$$
  
 $[\text{LiAl}_2(\text{OH})_6]\text{OH} \cdot 2\text{H}_2\text{O} + \text{Al}(\text{OH})_3 + 14\text{OH}^-$  (17)

As shown in Fig. S1 in Supplementary Materials (SM), the strongest crystal orientations of AlLi-LDH with space group *P*32 are the (003), (006), (112), (115), and (118), with the (003) plane

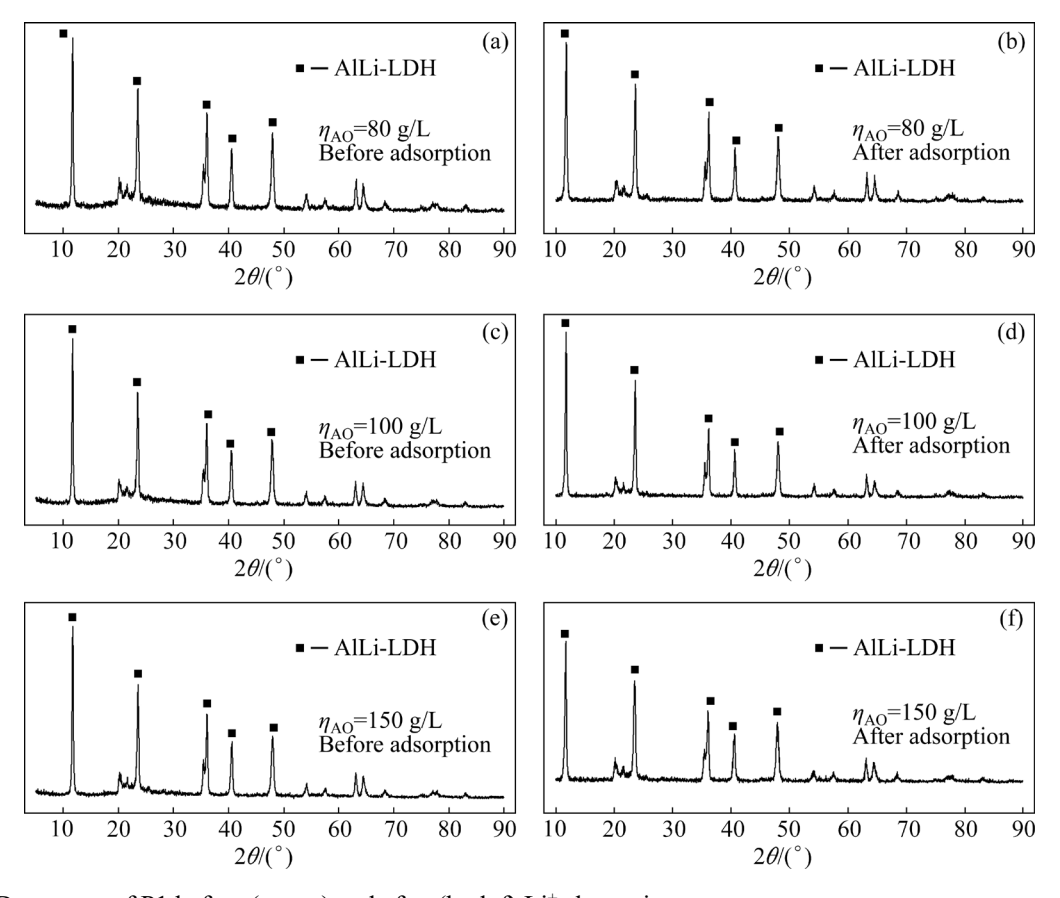


Fig. 2 XRD patterns of P1 before (a, c, e) and after (b, d, f) Li<sup>+</sup> absorption

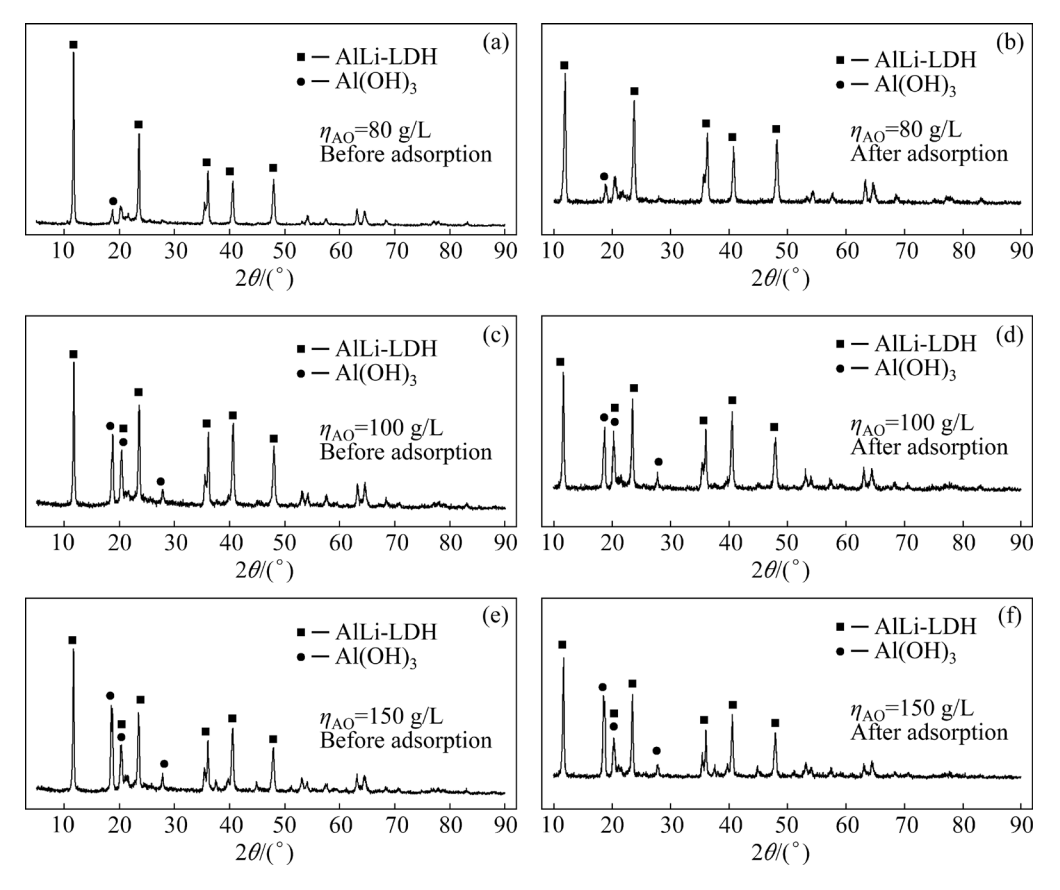


Fig. 3 XRD patterns of P2 before  $(a,\,c,\,e)$  and after  $(b,\,d,\,f)$   $Li^+$  absorption

being most prominent. The (001), (002), ( $\overline{1}31$ ), and (132) planes correspond to crystal orientations of AlLi-LDH in space group C2/m, where the highest peak is observed for the (001) crystal orientation. The characteristic peaks of AlLi-LDH in the products match well with the peaks of cards 81-1573 and 31-0704. However, it is difficult to determine whether the characteristic peak at  $2\theta$ =11.72° represents (003) or (001) crystal orientation. It is also difficult to assign the crystal orientation of the characteristic peaks at  $2\theta$ =23.60° and 36.04°. The Le Bail fitting method was used to

analyze the XRD patterns to determine the structural characteristics of P1 and P2. The initial crystal structure information of AlLi-LDH is obtained from cards 81-1573 and 31-0704. The analysis results are shown in Figs. S2 and S3 in SM. The Chi2 values are all approximately 2.00, suggesting a good fit. According to the Le Bail fitting results, AlLi-LDH crystallizes in both the *P*32 and *C*2/*m* space groups, as shown in Figs. 4(a) and 5(a). Before the Li<sup>+</sup> adsorption, the main orientations of *P*32-type AlLi-LDH are (006), (112), (115), and (118), whereas the main orientations of

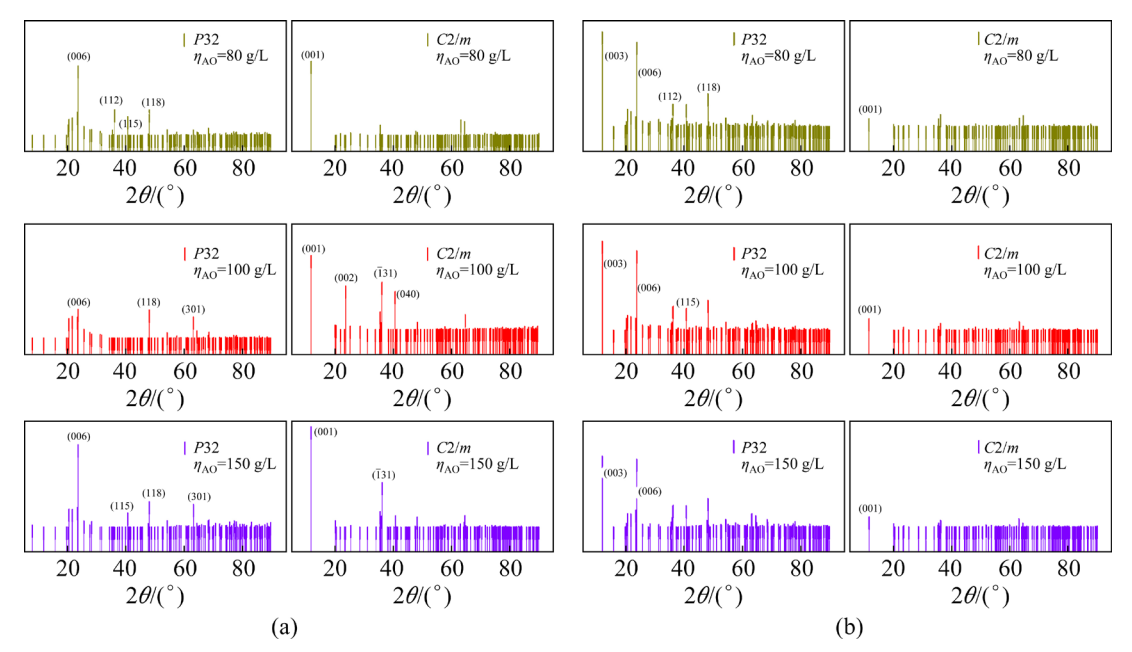


Fig. 4 Le Bail fitting data of P1: (a) Before adsorption; (b) After adsorption

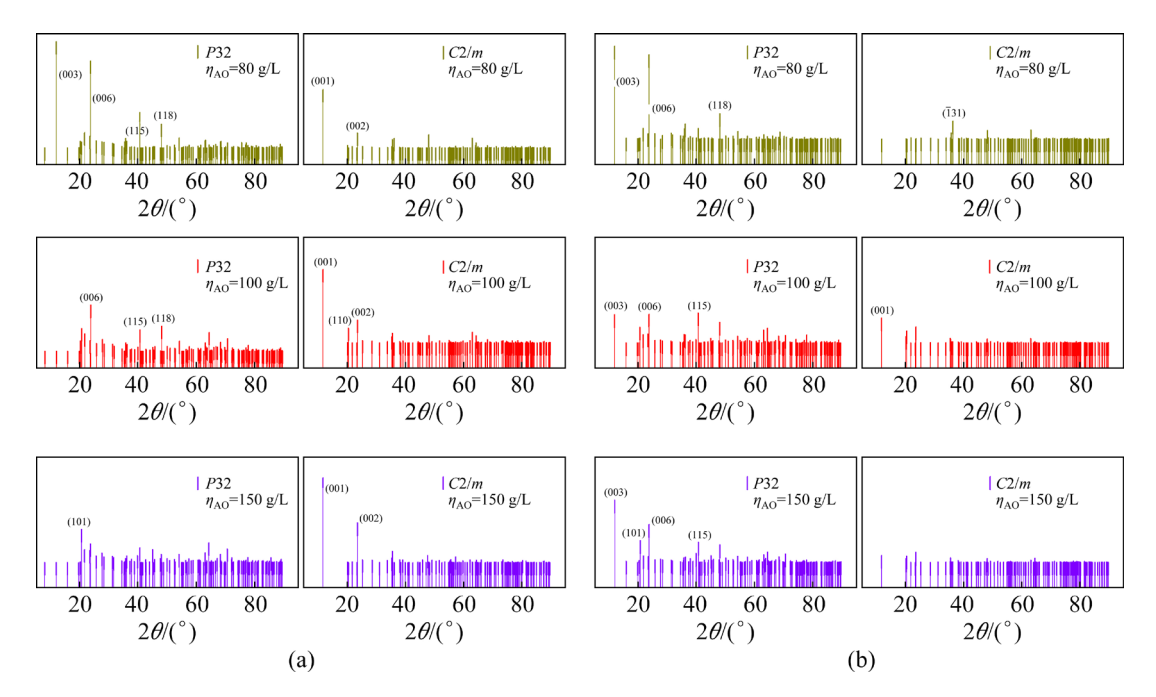


Fig. 5 Le Bail fitting data of P2: (a) Before adsorption; (b) After adsorption

C2/m-type AlLi-LDH are (001), (002), and ( $\overline{1}31$ ). The characteristic peaks of C2/m-type AlLi-LDH clearly became less intense after the Li<sup>+</sup> adsorption.

Table S1 in SM gives the lattice parameters from cards 81-1573 and 31-0704. The Le Bail fitting results for the lattice parameters are given in Tables S2 and S3 in SM. To clarify this variation, maps are used to display the cell volumes. The *P*32-type AlLi-LDH is represented by P1-LDH1 and P2-LDH1. P1-LDH2 and P2-LDH2 represent AlLi-LDH with space group *C*2/m. The cell volumes of LDH1 (P1-LDH1, P2-LDH1) and LDH2 (P1-LDH2, P2-LDH2) are shown in Figs. 6(a) and

6(b), respectively. The cell volumes of P1-LDH1, P1-LDH2, P2-LDH1, and P2-LDH2 decrease after the Li<sup>+</sup> adsorption when  $\eta_{AO}$  are 80, 100, and 150 g/L, respectively. Al(OH)<sub>3</sub> with space group of C2/m and P-1 of P2 is represented by P2-AH1 and P2-AH2, respectively. The Le Bail fitting results for the lattice parameters of Al(OH)<sub>3</sub> are shown in Table S4, Figs. S4, and S5 in SM. The calculated results are similar to the values from the standard cards (Fig. S6 and Table S5 in SM). The cell volume of Al(OH)<sub>3</sub> also decreases after the Li<sup>+</sup> adsorption. Thus, Al(OH)<sub>3</sub> can also adsorb lithium ions.

The full XPS profile of AlLi-LDH (P1,  $\eta_{AO}$ = 150 g/L) is shown in Fig. 7(a). The Al 2p, O 1s,

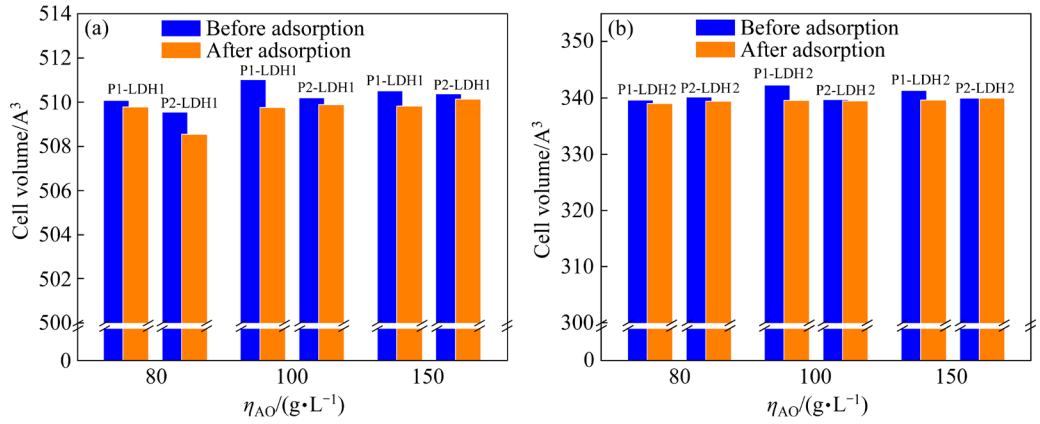


Fig. 6 Cell volumes of LDH1 (a) and LDH2

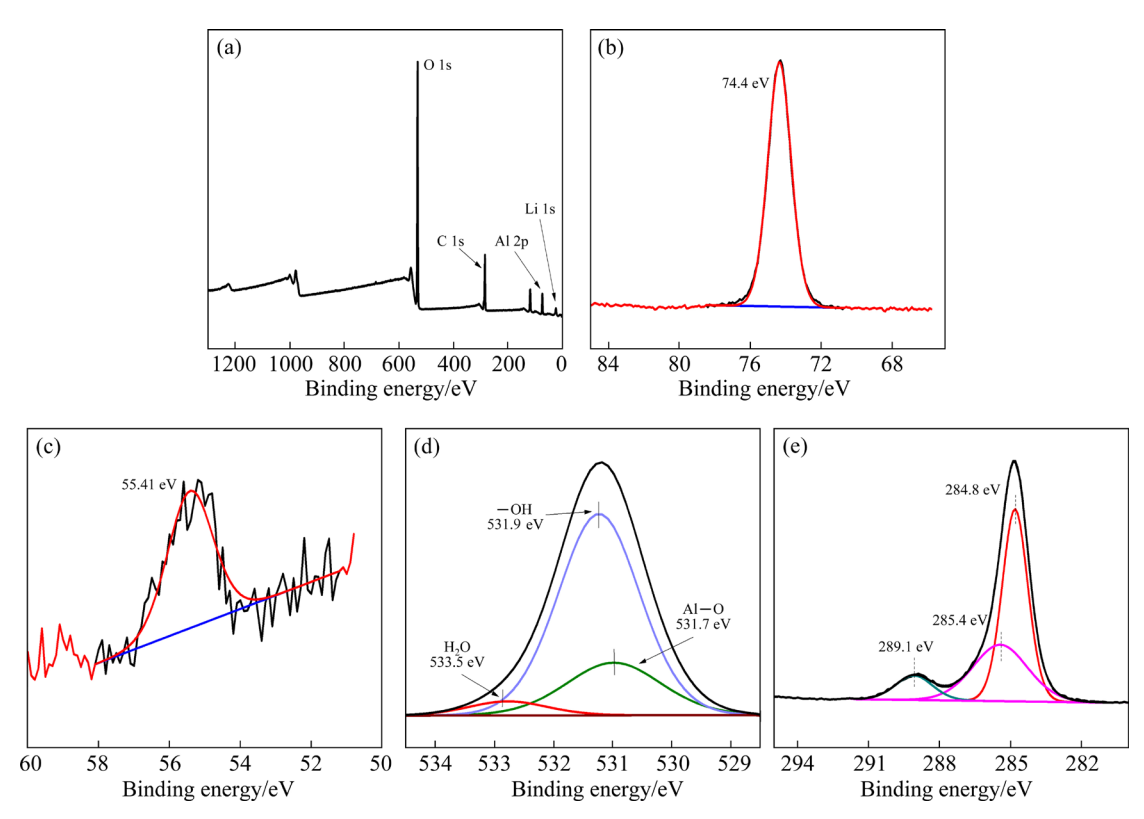


Fig. 7 XPS analysis results of AlLi-LDH: (a) Over-view; (b) Al 2p; (c) Li 1s; (d) O 1s; (e) C 1s

C 1s, and O 1s peaks indicate the successful synthesis of AlLi-LDH. Figure 7(b) presents a peak at 74.4 eV which is assigned to the characteristic peak of Al 2p. The characteristic Li 1s peak is shown in Fig. 7(c). The O 1s spectrum (Fig. 7(d)) is split into three peaks: the peak at 531.7 eV is a characteristic metal—O peak (Al—O and Li—O); the peak at 531.9 eV is characteristic peak of the hydroxyl (-OH) group; the peak at 533.5 eV is a characteristic peak of H<sub>2</sub>O. The C 1s spectrum (Fig. 7(e)) is divided into three peaks: the peak at 284.8 eV is assigned to the C—C bond of aliphatic carbon, the peak at 285.4 eV is assigned to the C—O bond, and the peak at 289.1 eV is assigned to the C=O (CO<sub>2</sub>) group. The presence of C-O and C=O bonds indicates the presence of  $CO_3^{2-}$  in AlLi-LDH. The generation of CO<sub>3</sub><sup>2-</sup> may be due to reactions between the interlayer hydroxide ions and  $CO_2$  in the air.

#### 3.2 Microstructural characteristics of AlLi-LDH

The microstructure of P1 is shown in Fig. 8 when  $\eta_{AO}$  values are 80, 100, and 150 g/L. The P1 particles have consistent shapes and sizes comprising micrometer-sized spheres of approximately 5–10  $\mu$ m in diameter. Clusters of microspheres are formed by agglomeration. The microstructure of P1 does not change after the Li<sup>+</sup> adsorption.

The TEM images are shown in Fig. 9. The layer stacking phenomenon becomes more apparent after adsorption, where the crystalline grains display a hexagonal structure (Figs. 9(b, e)). As evidenced by the Le Bail fitting results, AlLi-LDH

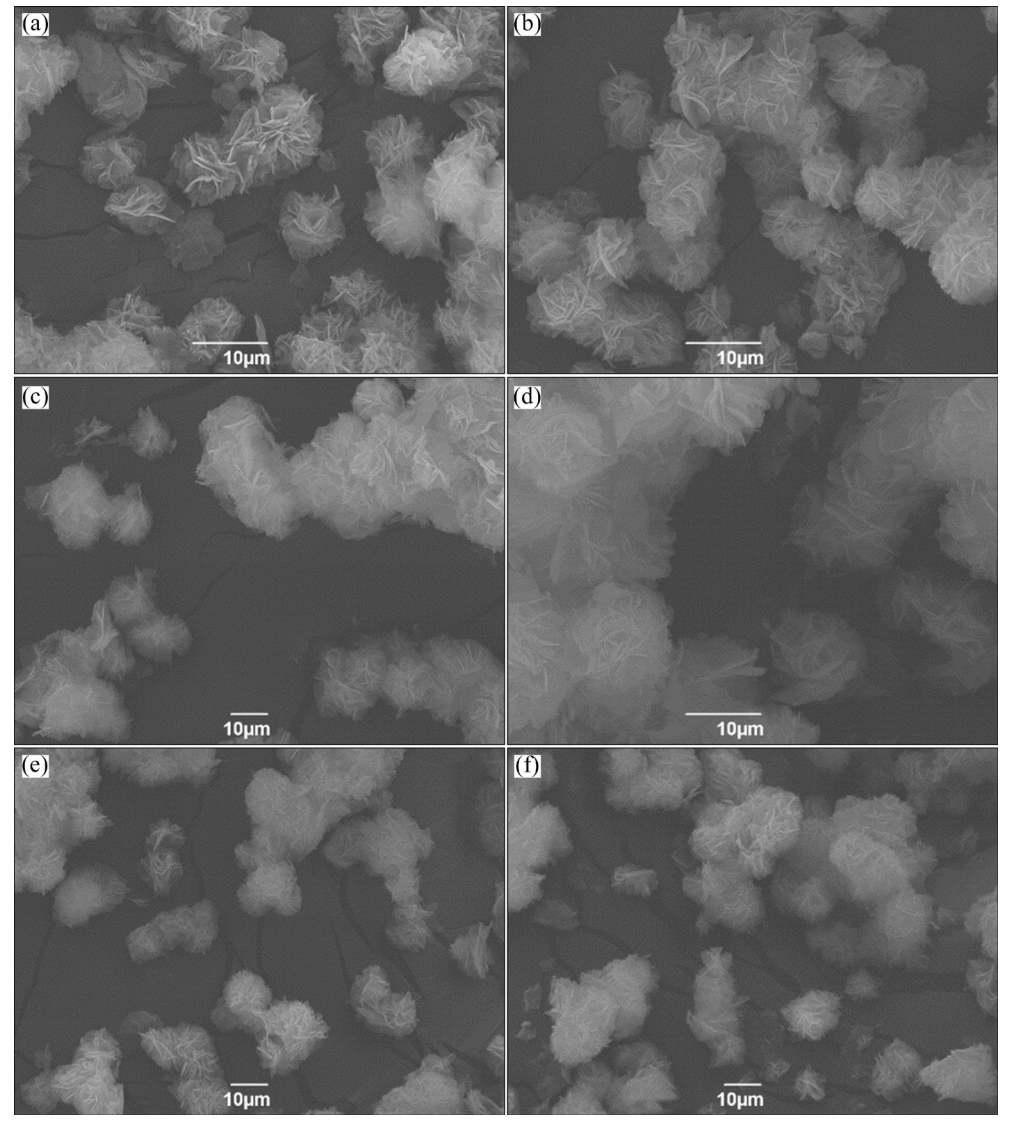


**Fig. 8** SEM images of P1 synthesized with different  $\eta_{AO}$ : (a) 80 g/L, before adsorption; (b) 80 g/L, after adsorption; (c) 100 g/L, before adsorption; (d) 100 g/L, after adsorption; (e) 150 g/L, before adsorption; (f) 150 g/L, after adsorption

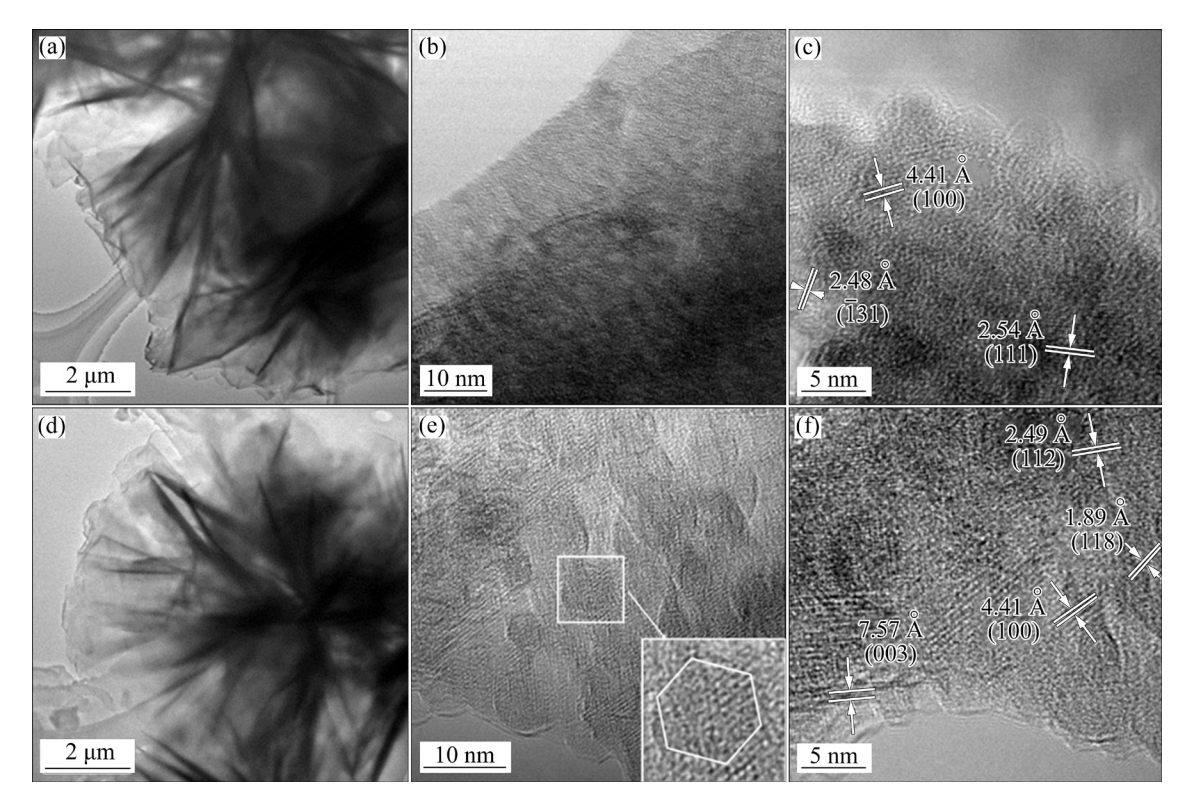


Fig. 9 HRTEM images of AlLi-LDH (P1,  $\eta_{AO}$ =150 g/L): (a, b, c) Before adsorption; (d, e, f) After adsorption

transforms from C2/m-type (81-1573) to P32-type (31-0704) after the Li<sup>+</sup> adsorption. As shown in Figs. 9(c, f), the interlayer spacings of crystal orientations ( $\overline{1}31$ ) of 81-1573, (111) of 81-1573, and (100) of 31-0704 are 2.48, 2.54, and 4.41 Å, respectively. The interlayer spacings of crystal orientations (003), (100), (118), and (112) of 31-0704 are 7.57, 4.41, 1.89, and 2.49 Å, respectively.

## 3.3 Adsorption performance of AlLi-LDH

The Li<sup>+</sup> adsorption curve with P1-LDH for time ranging from 10 min to 48 h in a pure lithium solution is shown Fig. 10; the kinetic analysis results are shown in Fig. 11. After adsorption for 48 h, the Li<sup>+</sup> adsorption amount was 16.50 mg/g. The correlation coefficient ( $R^2$ ) represents the matching degree between the adsorption process and model. For the Li<sup>+</sup> adsorption by P1-LDH, the  $R^2$  of the second-order adsorption model is greater than that of the first-order adsorption model. The adsorption capacity predicted by applying the second-order adsorption model is 17.57 mg/g, which is slightly higher than the adsorption amount at 48 h. However, the Li<sup>+</sup> adsorption capacity predicted by the first-order adsorption model is

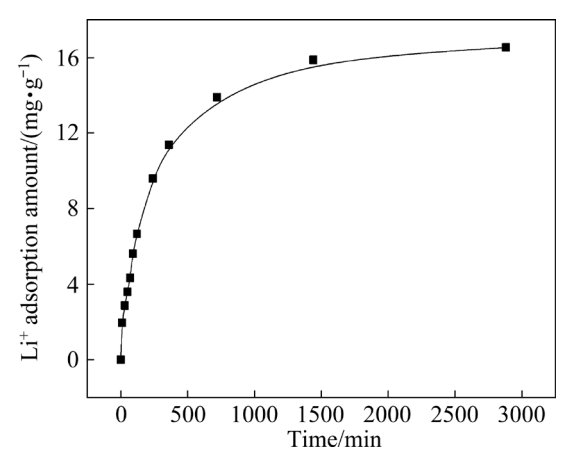
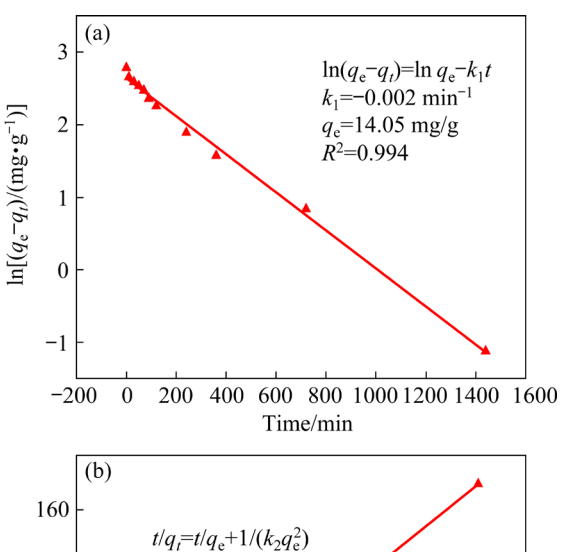
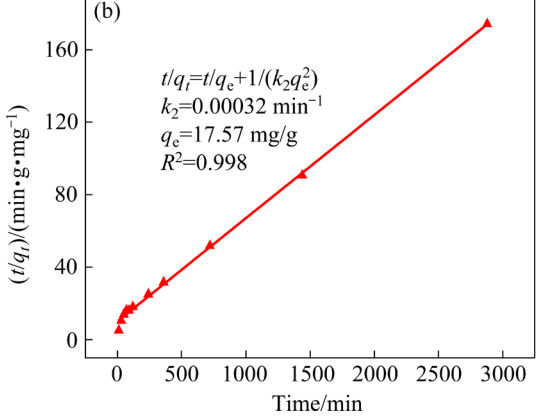


Fig. 10 Lithium adsorption curve by P1-LDH in pure lithium solution

14.05 mg/g, which is much smaller than that at 48 h. Therefore, the P1-LDH adsorption process can be described by the pseudo-second-order model, which suggests that the adsorption efficiency is controlled by the chemical adsorption process.

A mixed solution of LiCl and MgCl<sub>2</sub> with initial Mg<sup>2+</sup> and Li<sup>+</sup> concentrations of 101.8 g/L and 95.4 mg/L, respectively, was prepared, where the mass ratio ( $\beta_{\rm Mg}^{\rm Li}$ ) was 1067. The amount of lithium ions adsorbed by the added AlLi-LDH is 1.23 times the total amount of lithium ions in the solution





**Fig. 11** Fitting curves of kinetics models for Li<sup>+</sup> adsorption process by P1-LDH: (a) Pseudo-first-order; (b) Pseudo-second-order

(Table 1). At adsorption time of 1, 2, 4, and 24 h, the Li<sup>+</sup> adsorption efficiencies are 59.88%, 56.78%, 57.63%, and 58.50%, respectively. The amount of Li<sup>+</sup> adsorbed is in the range of 8.51–8.98 mg/g when the adsorption time is extended from 1 to 24 h. Thus, the maximum Li<sup>+</sup> adsorption amount is reached within 1 h under the current experimental conditions. After an adsorption time of 1 h, the Mg<sup>2+</sup> adsorption amount is 0.87 mg/g and the  $\beta_{M\sigma}^{Li}$  of the final solution is 0.10. The Mg<sup>2+</sup>/Li<sup>+</sup> separation effect is the best at this time and the separation coefficient  $\alpha_{\mathrm{Mg}^{2+}}^{\mathrm{Li}^{+}}$  is 29536. When the adsorption time is extended to 24 h, the Mg2+ adsorption amount increases to 0.37 mg/g and the separation coefficient decreases to 7505. Thus, the extension of adsorption time can promote the Mg<sup>2+</sup> adsorption and decrease the separation effect of Mg<sup>2+</sup>/Li<sup>+</sup>. The adsorption amount of AlLi-LDH in Fig. 10 is different with the data in Table 1. The difference may be caused by the concentrations of Li<sup>+</sup> and impurity ions in the solution.

**Table 1** Results of separation experiments

| Time/h | $q_t^{\mathrm{Li}^+}/(\mathrm{mg}\cdot\mathrm{g}^{-1})$ | $q_t^{\mathrm{Mg}^+}/(\mathrm{mg}\cdot\mathrm{g}^{-1})$ | $lpha_{\mathrm{Mg}^{2^{+}}}^{\mathrm{Li}^{+}}$ | $\beta_{\rm Mg^{2^+}}^{\rm Li^+}$ |
|--------|---|---|--|-----------------------------------|
| 1      | 8.98  | 0.87  | 29536  | 0.10                              |
| 2      | 8.51  | 3.26  | 6883   | 0.38                              |
| 4      | 8.64  | 3.87  | 6024   | 0.45                              |
| 24     | 8.77  | 3.22  | 7505   | 0.37                              |

#### 3.4 Interaction analysis of Li-O in AlLi-LDH

AlLi-LDH with space group C2/m is a monoclinic crystal system, whereas the P32 congener is hexagonal. The lithium ion is located at the center of the aluminum-oxygen octahedral structure and interacts with six surrounding hydroxide ions constituted by O<sub>49</sub>, O<sub>50</sub>, O<sub>51</sub>, O<sub>52</sub>,  $O_{53}$ , and  $O_{54}$ , as shown in Figs. 12(a, b). The IGM method is originally proposed based on promolecular density. Thus, it can be used to analyze the interactions according to the geometric structure information of cards 81-1573 and 31-0704. The Al-O-Li structural unit and IGM data are shown in Figs. 12(c, d). These interactions can be divided into three types: strong electrostatic interactions (blue), van der Waals interactions (green), and strong repulsive interactions (steric effect, red). As shown in Table 2, Li—O bond length is 2.095 Å in P32-type AlLi-LDH. The interaction strength among the central lithium ion and the surrounding six hydroxide ions are almost the same. This

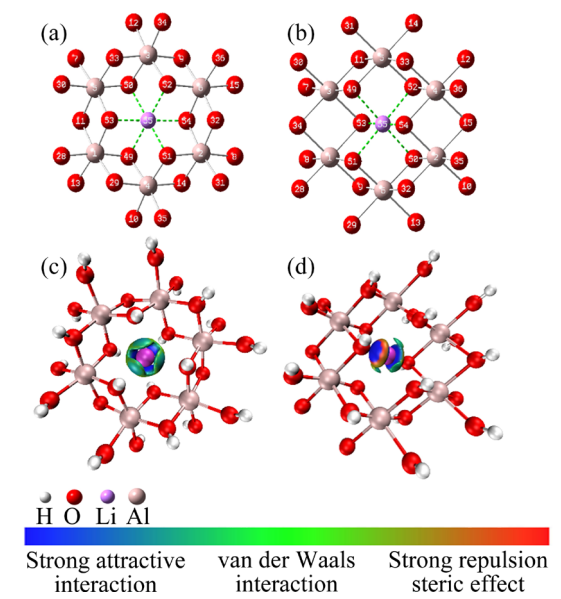


**Fig. 12** Crystal structure and IGM analysis results for LDH1 and LDH2: (a) LDH1, hexagonal, *P*32; (b) LDH2, monoclinic, *C*2/*m*; (c) IGM for LDH1; (d) IGM for LDH2

| Space group | Li <sub>55</sub> —O <sub>49</sub> | Li <sub>55</sub> —O <sub>50</sub> | Li <sub>55</sub> —O <sub>51</sub> | Li <sub>55</sub> —O <sub>52</sub> | Li <sub>55</sub> —O <sub>53</sub> | Li <sub>55</sub> —O <sub>54</sub> |
|-------------|-----------------------------------|-----------------------------------|-----------------------------------|-----------------------------------|-----------------------------------|-----------------------------------|
| C2/m        | 2.281                             | 2.281                             | 2.281                             | 2.281                             | 1.523                             | 1.523                             |
| P32         | 2.095                             | 2.095                             | 2.095                             | 2.095                             | 2.095                             | 2.095                             |

Table 2 Li—O bond lengths of AlLi-LDH with monoclinic (C2/m) and hexagonal (P32) crystal systems (Å)

interaction is attributed to the electrostatic effect. The Li—O bond lengths are 2.281 and 1.523 Å when the space group is C2/m. Owing to the shorter distance,  $\text{Li}_{55}$ — $\text{O}_{53}^{C2/m}$  and  $\text{Li}_{55}$ — $\text{O}_{54}^{C2/m}$  have greater interaction strengths than  $\text{Li}_{55}$ — $\text{O}_{50}^{C2/m}$ ,  $\text{Li}_{55}$ — $\text{O}_{51}^{C2/m}$ , and  $\text{Li}_{55}$ — $\text{O}_{52}^{C2/m}$ . The red region stands for the steric effect between the central lithium ion and hydrogen atoms of the hydroxide ions, which are located around the blue region.

As shown in Table 3, Li-O forms tetrahedral or octahedral structures in lithium aluminate, with bond lengths of 1.897-1.948 Å and 2.043 Å, respectively. The Li-O bond in the tetrahedral structure is shorter, and the interaction is stronger. The bond length of  $\text{Li}_{55}$ — $\text{O}_{49}^{P32}$  is longer than that of lithium aluminate, which suggests that the interaction strength of Li-O is weaker in AlLi-LDH with space group P32. Consequently, lithium ions can be leached by the hot water washing. However, the bond lengths of  $\text{Li}_{55}$ — $O_{53}^{C2/m}$  and  $\text{Li}_{55}$ — $O_{54}^{C2/m}$  are even shorter than those of Li—O in lithium aluminate. Therefore, the interactions of  $\text{Li}_{55}$ — $\text{O}_{53}^{C2/m}$  and  $\text{Li}_{55}$ — $\text{O}_{54}^{C2/m}$  are the strongest, which suggests that it is more difficult for Li+ to be inserted into the cavity formed by  $O_{53}^{C2/m}$  and  $O_{54}^{C2/m}$ . It is also difficult to remove  $Li^+$  ions from this cavity. Thus, compared with C2/m-type AlLi-LDH, the Li<sup>+</sup> adsorption and desorption are easier in P32-type AlLi-LDH.

**Table 3** Li — O bond lengths of lithium aluminate structures in different ICSD cards (Å)

| ICSD card No. | Li—O       |             |  |  |
|---------------|------------|-------------|--|--|
| icsb card no. | Octahedral | Tetrahedron |  |  |
| 1037          | _          | 1.936       |  |  |
| 10480         | 2.043      | _           |  |  |
| 16229         | _          | 1.897       |  |  |
| 23815         | _          | 1.948       |  |  |
| 30249         | _          | 1.941       |  |  |

#### 4 Conclusions

(1) AlLi-LDH was synthesized through the

co-precipitation of lithium ions and aluminate anions. Pure AlLi-LDH can be synthesized by dropping lithium hydroxide solution into the sodium aluminate solution.

- (2) The AlLi-LDH particles exhibit consistent shapes and sizes. The diameters of the microspheres vary from 5 to 10 μm. The microstructure is unaffected by the Li<sup>+</sup> adsorption. AlLi-LDH can crystallize in both *P*32 and *C*2/m space groups, and is fully transformed into the *P*32-type structure after the Li<sup>+</sup> adsorption.
- (3) Li<sup>+</sup> is more easily inserted into the center of the Al–O octahedral structure when the space group is *P*32. The interaction of Li –O in *P*32-type AlLi-LDH occurs via an electrostatic effect.
- (4) The amount of  $\text{Li}^+$  adsorbed after 1 h is 8.98 mg/g, with  $Mg^{2^+}/\text{Li}^+$  separation coefficient of 29536 when the mass ratio of  $Mg^{2^+}$  to  $\text{Li}^+$  is 1067. The  $\text{Li}^+$  adsorption capacity of AlLi-LDH is 16.50 mg/g when the absorption time is extended to 24 h.

#### CRediT authorship contribution statement

Yong-pan TIAN: Conceptualization, Methodology, Software, Investigation, Formal analysis, Writing — Original draft; Cheng-cheng WANG: Data curation, Writing — Original draft; Fan ZHANG: Visualization, Investigation, Software; Liang XU: Resources, Supervision, Validation; Zhuo ZHAO: Conceptualization, Funding acquisition, Resources, Supervision, Writing — Review & editing; Bi-hai TONG: Visualization, Writing — Review & editing.

#### **Declaration of competing interest**

The authors declare that they have no known competing financial interests or personal relationships that could have appeared to influence the work reported in this paper.

## Acknowledgments

The authors are grateful for the financial supports from the National Natural Science Foundation of China (Nos. 51704011, 51904003), and the Joint Funds of the National Natural Science Foundation of China (No. U1703130).

## **Supplementary Materials**

Supplementary Materials in this paper can be found at: http://tnmsc.csu.edu.cn/download/22-p1321-2022-1057-Supplementary\_Materials.pdf.

#### References

- [1] ZHANG Ye, SUN Wei, XU Rui, WANG Li, TANG Hong-hu. Lithium extraction from water lithium resources through green electrochemical-battery approaches: A comprehensive review [J]. Journal of Cleaner Production, 2021, 285: 124905.
- [2] REN Guo-xing, LIAO Cai-bin, LIU Zhi-hong, XIAO Song-wen. Lithium and manganese extraction from manganese-rich slag originated from pyrometallurgy of spent lithium-ion battery [J]. Transactions of Nonferrous Metals Society of China, 2022, 32: 2746–2756.
- [3] CAO Ning, ZHANG Ya-li, CHEN Lin-lin, JIA Yun, HUANG Yao-guo. Priority recovery of lithium and effective leaching of nickel and cobalt from spent lithium-ion battery [J]. Transactions of Nonferrous Metals Society of China, 2022, 32: 1677–1690.
- [4] AN J W, KANG D J, TRAN K T, KIM M J, LIM T, TRAN T. Recovery of lithium from Uyuni salar brine [J]. Hydrometallurgy, 2012, 117/118: 64-70.
- [5] SUN Shu-ying, CAI Li-juan, NIE Xiao-yao, SONG Xing-fu, YU Jian-guo. Separation of magnesium and lithium from brine using a Desal nanofiltration membrane [J]. Journal of Water Process Engineering, 2015, 7: 210–217.
- [6] HE Mao-yong, LUO Chong-guang, YANG Hong-jun, KONG Fan-cui, LI Yu-long, DENG Li, ZHANG Xi-ying, YANG Kai-yuan. Sources and a proposal for comprehensive exploitation of lithium brine deposits in the Qaidam Basin on the northern Tibetan Plateau, China: Evidence from Li isotopes [J]. Ore Geology Reviews, 2020, 117: 103277.
- [7] CHEN Jun, LIN Sen, YU Jian-guo. High-selective cyclic adsorption and magnetic recovery performance of magnetic lithium-aluminum layered double hydroxides (MLDHs) in extracting Li<sup>+</sup> from ultrahigh Mg/Li ratio brines [J]. Separation and Purification Technology, 2021, 255: 117710.
- [8] ZHANG Jian, LIU Ya-hui, LIU Wen-sen, WANG Li-na, CHEN Jing, ZHU Zhao-wu, QI Tao. Mechanism study on the synergistic effect and emulsification formation of phosphine oxide with β-diketone for lithium extraction from alkaline systems [J]. Separation and Purification Technology, 2021, 279: 119648.
- [9] ZHAO Xiao-yu, YANG Hao-cun, WANG Yan-fei, YANG Li-bin, ZHU Liang. Lithium extraction from brine by an asymmetric hybrid capacitor composed of heterostructured lithium-rich cathode and nano-bismuth anode [J]. Separation and Purification Technology, 2021, 274: 119078.
- [10] CHUNG K, LEE J, KIM W, KIM S, CHO K. Inorganic adsorbent containing polymeric membrane reservoir for the recovery of lithium from seawater [J]. Journal of Membrane Science, 2008, 325: 503–508.
- [11] ZHONG Jing, LIN Sen, YU Jian-guo. Lithium recovery from ultrahigh Mg<sup>2+</sup>/Li<sup>+</sup> ratio brine using a novel granulated

- Li/Al-LDHs adsorbent [J]. Separation and Purification Technology, 2021, 256: 117780.
- [12] ZHONG Jing, LIN Sen, YU Jian-guo, Effects of excessive lithium deintercalation on Li<sup>+</sup> adsorption performance and structural stability of lithium/aluminum layered double hydroxides [J]. Journal of Colloid and Interface Science, 2020, 572: 107–113.
- [13] THIEL J P, CHIANG C K, POEPPELMEIER K R. Structure of lithium aluminum hydroxide dihydrate (LiAl<sub>2</sub>(OH)<sub>7.2</sub>H<sub>2</sub>O) [J]. Chemistry of Materials, 2002, 5: 297–304.
- [14] CHAMPENOIS J B, MESBAH A, DANNOUX-PAPIN A, COUMES C C D, DACHEUX N. LiAl<sub>2</sub>(OH)<sub>6</sub>OH<sub>.2</sub>H<sub>2</sub>O solubility product and dihydrogen radiolytic production rate under γ-irradiation [J]. Journal of Nuclear Materials, 2018, 508: 92–99.
- [15] ZHANG Yue-ping, CHENG Xi-yue, WU Chen, KÖHLER Jürgen, DENG Shui-quan. Electronic structure and lithium diffusion in LiAl<sub>2</sub>(OH)<sub>6</sub>Cl studied by first principle calculations [J]. Molecules, 2019, 24: 2667.
- [16] JUAN R C. Recent advances in magnetic structure determination by neutron powder diffraction [J]. Physica B: Condensed Matter, 1993, 192: 55-69.
- [17] BRITTO S, KAMATH P V. Polytypism in the lithium–aluminum layered double hydroxides: The [LiAl<sub>2</sub>(OH)<sub>6</sub>]<sup>+</sup> layer as a structural synthon [J]. Inorganic Chemistry, 2011, 50: 5619–5627.
- [18] BESSERGUENEV A V, FOGG A M, FRANCIS R J, PRICE S J, O'HARE D, ISUPOV V P, TOLOCHKO B P. Synthesis and structure of the gibbsite intercalation compounds (LiAl<sub>2</sub>(OH)<sub>6</sub>)X (X: Cl, Br, NO<sub>3</sub>) and (LiAl<sub>2</sub>(OH)<sub>6</sub>)Cl·H<sub>2</sub>O using synchrotron X-ray and neutron powder diffraction [J]. Chemistry of Materials, 1997, 9: 241–247.
- [19] WILLIAMS G R, MOORHOUSE S J, PRIOR T J, FOGG A M, REES N H, O'HARE D. New insights into the intercalation chemistry of Al(OH)<sub>3</sub> [J]. Dalton Transactions, 2011, 40: 6012.
- [20] PARANTHAMAN M P, LI Ling, LUO Jia-qi, HOKE T, UCAR H, MOYER B A, HARRISON S. Recovery of lithium from geothermal brine with lithium-aluminum layered double hydroxide chloride sorbents [J]. Environmental Science & Technology, 2017, 51: 13481– 13486.
- [21] LI Yuan-yuan, TANG Na, ZHANG Lei, LI Jia. Fabrication of Fe-doped lithium-aluminum-layered hydroxide chloride with enhanced reusable stability inspired by computational theory and its application in lithium extraction [J]. Colloids and Surfaces A: Physicochemical and Engineering Aspects, 2022, 658: 130641.
- [22] OGAWA Y, KOIBUCHI H, SUTO K, INOUE C. Effects of the chemical compositions of Salars de Uyuni and Atacama brines on lithium concentration during evaporation [J]. Resource Geology, 2014, 64: 91–101.
- [23] XU Li, ZENG Xian-jie, HE Qing, DENG Tao, ZHANG Cheng-yi, ZHANG Wen. Stable ionic liquid-based polymer inclusion membranes for lithium and magnesium separation [J]. Separation and Purification Technology, 2022, 288: 120626.
- [24] KHALIL A, MOHAMMED S, HASHAIKEH R, HILAL N. Lithium recovery from brine: Recent developments and

- challenges [J]. Desalination, 2022, 528: 115611.
- [25] XU Ping, HONG Jun, QIAN Xiao-ming, XU Zhi-wei, XIA Hong, TAO Xu-chen, XU Zhen-zhen, NI Qing-qing. Materials for lithium recovery from salt lake brine [J]. Journal of Materials Science, 2021, 56: 16-63.
- [26] CHEN Jun, LIN Sen, YU Jian-guo. Quantitative effects of Fe<sub>3</sub>O<sub>4</sub> nanoparticle content on Li<sup>+</sup> adsorption and magnetic recovery performances of magnetic lithium-aluminum layered double hydroxides in ultrahigh Mg/Li ratio brines [J]. Journal of Hazardous Materials, 2020, 388: 122101.
- [27] LEFEBVRE C, KHARTABIL H, BOISSON J C, CONTRERAS GARCÍA J, PIQUEMAL J P, HÉNON E. The independent gradient model: A new approach for probing strong and weak interactions in molecules from wave function calculations [J]. ChemPhysChem, 2018, 19: 724-735.
- [28] LU Tian, CHEN Qin-xue. Independent gradient model based on Hirshfeld partition: A new method for visual study of interactions in chemical systems [J]. Journal of Computational Chemistry, 2022, 43: 539–555.
- [29] LU Tian, CHEN Fei-wu. Multiwfn: A multifunctional wavefunction analyzer [J]. Journal of Computational Chemistry, 2012, 33: 580–592.
- [30] WILLIAM H, ANDREW D, KLAUS S. VMD: Visual molecular dynamics [J]. Journal of Molecular Graphics, 1996, 14: 33–38.
- [31] HUA Zhong-sheng, WU Xiao-bin, ZHU Zeng-li, HE Ji-wen, HE Shi-wei, LIU Huan, XU Liang, YANG Yong-xiang, ZHAO Zhuo. One-step controllable fabrication of 3D structured self-standing Al<sub>3</sub>Ni<sub>2</sub>/Ni electrode through molten salt electrolysis for efficient water splitting [J]. Chemical Engineering Journal, 2022, 427: 131743.

# AlLi-LDH 中 Al-O 八面体环吸附锂的机制

田勇攀, 王成成, 张 帆, 徐 亮, 赵 卓, 童碧海

安徽工业大学 冶金工程学院, 马鞍山 243032

摘 要:采用共沉淀法合成铝锂层状双氢氧化物(AlLi-LDH)并进行提锂试验。AlLi-LDH 的空间群为 P32 或 C2/m,微观形貌呈直径为  $5\sim10~\mu m$  的规则球形。AlLi-LDH 吸附  $Li^+$ 后,空间群转化为 P32。当  $Li^+$ 浓度为 95.4~m g/L时,1~h 后锂吸附量为 8.98~m g/g;吸附 48~h 后,吸附量增加到 16.50~m g/g;根据二级吸附模型预测  $Li^+$ 吸附总量为 17.57~m g/g。当  $Mg^{2+}/Li^+$ 的质量比为 1067~m , $Mg^{2+}/Li^+$ 分离系数为 29536。空间群为 P32~m ,Li-O 的相互作用强度变弱,且相互作用属于静电效应。具有 P32~m 空间基团的 AlLi-LDH 更容易吸附和解吸  $Li^+$ 。

关键词:共沉淀;铝锂层状双氢氧化物;空间群;吸附;锂

(Edited by Bing YANG)